IJRCE

ISSN 2248-9649

International Journal of

Research in Chemistry and Environment

Available online at: www.ijrce.org

Research Paper

Insoluble Biopolymer Based Metal Oxide Nanocomposites as Matrix for Enzyme Immobilization

***Anjali Krishna G., Geetha G., Savitha D. P. and Mohanan P. V.**
Department of Applied Chemistry, Cochin University of Science and Technology, INDIA

(Received 03rd March 2021 Accepted 31st March 2021)

Abstract: *Microbial α-amylase obtained as a result of screening of Bacillus subtilis strains can improve the breakdown of heavier biopolymers into simple sugar units. Insoluble chitosan-MnO_2 (CH-MnO_2, S1) and chitosan-NiO (CH-NiO, S2) nanocomposites were synthesised as a matrix for the adsorption of α-amylase and facilitate industrial applications. The physico-chemical characterizations of the synthesised nanocomposites were successfully determined. The optimization of immobilization criteria's such as pH, temperature, contact time and concentration were noticed using Lowry's method. The comparison of efficiency of free enzyme with immobilized enzyme were carried out by finding out the activity using DNS method followed by the determination of properties of free enzyme and immobilized enzyme. The rate of activity of free and immobilized enzymes were compared on the basis on activity temperature relationship. The kinetic studies revealed that supports S1 and S2 showed higher K_m and lower V_m values in comparison with free enzyme. The obtained values for K_m and V_m for S1 and S2 are 1.6303 mg/mL, 54 μmolmg^{-1}min^{-1} and 1.2947 mg/mL, 44.8 μmolmg^{-1}min^{-1} respectively. Thermal stability studies showed that S1 and S2 can withstand maximum relative activity upto 65 °C respectively. The reusability of the immobilized enzymes S1 and S2 showed maximum retainity in relative activity after 8 cycles. Storage stability of immobilized enzymes S1 and S2 were checked weekly and observed good stability upto 56 % for S1 and 66 % for S2 respectively after 6 weeks. The immobilization efficiency calculated for S1 and S2 were 56 % and 82.5 % respectively. The obtained results arrived at a conclusion of having better immobilization efficiency of support S2 over S1.*

Keywords: α-amylase, DNS Method, Lowry's Method, Thermal Stability, Reusability.

Introduction

Enzymes are proteins with linear chain of amino acids but still struggle for its high cost, selectivity and sensitivity so as to take a serious look on its limitations and finally various techniques emerged along with convenient enzyme immobilization method to reuse the enzymes and improve its storage stability by preserving its catalytic efficiency. Enzyme immobilization has attracted a long range of interest among others because of its capability to hold enzymes via various holding forces. It gives extra stability, rapid termination of reactions, high activity towards broader range of pH and temperature[1-3]. The prime idea behind enzyme immobilization is to hinder the freedom of enzyme by fixing it to solid matrices or within a semi-permeable support material. It should be mild to protect enzyme from denaturation are several strategies for enzyme immobilization includes adsorption, covalent binding, ionic binding, cross linking, matrix entrapment and microencapsulation[4,5]. Within the limited advantages, physical adsorption is the simplest technique and which includes reversible surface interaction between carrier and enzyme without cause any damage to enzyme.

Selection of support as carrier medium for the loading of enzyme is of prime importance. Natural polymers, synthetic polymers, processed materials and natural materials can be selected as supports. But the studies revealed that a polymer alone cannot provide all the beneficial qualities so the idea of incorporating biopolymer with nanomaterial promises for potential

applications with lustre performance. A great dealings with mesoporous support with giant surface area and high porous volume has become the main target of recent highlights [6-11]. And the compound nanocomposites are nanoscopic fine particles so as to boost the performance of the pure compound and their ancient composites that notably appearance on resistance to thermal and chemical degradation, less thermal coefficients, resistance to shock hundreds, high mechanical strength and stability to extremes of temperature and hydrogen ion concentration conditions[12].

Among various biopolymers, chitosan (CH) attached with nanoparticles can have great influence in using as stabilizing agent due to its extraordinary properties like outstanding film-forming capacity, strength, non-toxicity, biocompatibility, high permeability, cost free or susceptibility to chemical makeovers. Many tries are created to boost the property of biopolymer by created structural modification using the incorporation of metal oxide nanoparticles[13]. Polymers are the good host for metal [14-17] and semiconductor[18-21] nanoparticles, and a concord nanocomposite showed excellent optical and electrical properties. The CH hoists amino and hydroxyl group which makes its good adsorbent for heavy metals and dyes[22,23]. The selected biopolymer, CH mixed with MnO_2 and NiO nanoparticles resulted in the formation of insoluble polymer based nanocomposite of advanced application. The polysaccharide containing unbranched β chains with novel properties incorporated with metal oxide nanoparticles made them studied for biosensors, tissue engineering, separation film, water treatment, agriculture, drug delivery and catalysis[24-27].

Manganese oxides (MnO_2) exhibited in different crystal structures and it is selected due to oxidation property, environmental friendly nature, high activity, low cost, ease of handling, and convenient preparation[28] and finds applications in batteries, sensors, molecular sieves, catalysts and adsorbents[29]. The simple use of metal oxide alone may cause agglomeration due to high surface energy and Van der Waals forces[30-33]. Hence modification of MnO_2 with polymers could be one of effective way to prevent aggregation and provide high surface area[34]. The other metal oxide NiO has recently attracted much attention due to its high isoelectric point (10.8) and interesting electrocatalytic, piezoelectric, photonic and tunable size dependent surface properties that make it as a suitable candidate for the immobilization of various biomolecules including, sRNA, DNA, antibodies and enzyme[35,36]. CH based NiO nanocomposite material experienced high surface, functionality and increased hydrophilicity.

The enzyme selected for immobilization is α-amylase (1,4-α-D-glucan- glucanohydrolase) which hydrolyses alpha bonds of large, alpha-linked polysaccharides, such as starch and glycogen, yielding simple sugar units like glucose and maltose. It is an endo enzyme probably found in human and mammals, which hydrolyse α-1,4 glycosidic linkages in amylase, amylopectin and glycogen[37].

The entitled work relies on insoluble biopolymer based metal oxide nanocomposites chitosan- MnO_2 (CH-MnO_2, S1) and chitosan-NiO (CH-NiO, S2) as matrix for α-amylase immobilization. Immobilization was done by physical adsorption method. The synthesised nanocomposites were characterized by FT-IR, FE-SEM, XRD, TG-DTG and EDAX analysis. Optimization of immobilization parameters such as pH, temperature, contact time and concentration were carried out and estimated the efficiency of immobilization on the basis of immobilization yield and relative activity. Determined the properties of immobilized enzyme and free enzyme and the results confirmed that the synthesised nanocomposites can be used as a good matrix for enzyme immobilization with better immobilization efficiency.

Materials and Methods

α-amylase was purchased from Himedia Laboratories Pvt. Ltd, Mumbai. Soluble Starch (potato) has been procured from S. D. Fine Chem. Ltd. Mumbai. Chitosan was acquired from Meron marine chemicals, Cochin. Manganese (II) nitrate tetrahydrate ($Mn(NO_3)_2.4H_2O$), Nickel (II) nitrate hexahydrate ($Ni(NO_3)_2.6H_2O$), Potassium hydroxide (KOH), Sodium hydroxide (NaOH) and acetic acid (CH_3COOH) were secured from Merck Co.

Synthesis of Nanocomposites

Chitosan-MnO_2 (S1) Nanocomposite

Method of preparation of CH-MnO_2 nanocomposite was selected from the reported literature[38]. MnO_2 nanoparticles were prepared by the calcination of $Mn(NO_3)_2.4H_2O$ at 350 °C at 2hr. MnO_2 (0.25g) was added to 100 mL of 1% (v/v) aqueous acetic acid, where MnO_2 ionized into Mn^{4+} cations. Afterwards, CH (1g) was added to this dispersion. The product was sonicated for 1 h. The Mn^{4+} ions coordinated with –OH and $–NH_2$ groups of CH chains and precipitated as CH-Mn-OH^{3+} when pH of the solution was increased to 10 by the slow addition of 1M NaOH. The stirring of the solution was continued until it became clear. The precipitate obtained was heated for 5 h at 80 °C and dried.

Chitosan-NiO (S2) Nanocomposite

Procedure was referred from the literature[39-42]. 0.5 M solution of $Ni(NO_3)_2.6H_2O$ was prepared. Add 0.2 M KOH solution drop wise with constant stirring at room

temperature until become alkaline. The green precipitate of nickel hydroxide ($Ni(OH)_2$) thus obtained was centrifuged followed by washing with distilled water until neutral pH reached. The precipitate obtained was dried at 80 °C for about 24 h resulting in the formation of a transparent viscous solution of nickel hydroxide it was carried out for calcination at 400 °C for 2 h to obtain black NiO nanoparticle. A NiO nanoparticle (5 mg) was dispersed in 10 mL of CH solution (0.50 %) in acetate buffer (0.05 M) with constant stirring at room temperature. Finally, a highly viscous solution of CH with uniformly dispersed NiO nanoparticles was obtained and dried it in vaccum oven.

Physico-Chemical Characterization of Nanocomposites

The organic and inorganic species with low content detected via FT-IR spectroscopy using Thermo Nicolet, Avatar 370 FT-IR spectrophotometer in the wavelength region 400-4000 cm^{-1}. The morphology of nanocomposite analysed with FE-SEM using SIGMA HV and VP series scanning electron microscope. The crystalline or amorphous nature of nanocomposite estimated with XRD using Bruker AXS D8 advance rotaflex diffraction meter. Thermal stability of the nanocomposite was evaluated by using Perkin Elmer Pyris Diamond 6 thermogravimetric analyser. Elemental analysis of a sample was done with EDX or EDXRF using JEOL-JSM 5800 machine.

Estimation of Protein in Immobilized Samples

Lowry's method was followed for the estimation of protein in the immobilised samples, S1 and S2. A calibration curve was plotted using different protein concentrations ranges from 0.1 to 1 mg/mL which were fixed as standard for the further studies. The immobilised enzyme along with different protein concentrations were incubated for 2 hour at room temperature followed by the addition of reagent C (mixture of A and B where A is 5 g Sodium carbonate in 250 mL standard flask and 0.1 N sodium hydroxide in 100 mL standard flask and B is 0.5 g Copper Sulphate penta hydrate and 1 g sodium potassium tartrate in 100 mL standard flask). A 0.5 mL Folin & Ciocalteus Phenol reagent was added to each sample and took absorbance at 660 nm in Thermo Scientific Evolution 201 UV-Vis Double beam spectrophotometer. The amount of protein in the supernatant solution was compared with control solution. Also sufficient amount of nanocomposites were shaken with 0.5 mg/mL enzyme solution in desired buffer at room temperature for exact immobilization. The immobilization factors like pH, temperature, contact time and protein concentration were optimized. The selected range of pH, temperature, contact time and protein concentration for immobilization taken as 4 to 9, 35 ^{0}C to 65 ^{0}C, 30-150 minutes and 0.2-1 mg/mL respectively. The resultant protein precipitate was separated by filtration and washed several times with same buffer solution. The supernatant solutions were carried for protein estimation. The residues were kept in a refrigerator at 4°C for detailed studies. Immobilization yield (IY) was calculated (Eq. (1)) from the difference in values of protein concentration in floating solution after and before immobilization (control).

$$IY\% = \frac{C_1 - C_2}{C_1} X\,100 \quad (1)$$

Where C_1 is the concentration of protein taken for immobilization and C_2 is the concentration of protein present in floating solution after immobilization.

Activity yield (AY) (Eq. (2)) was determined by noting the activity of immobilized enzyme and the activity of starting enzyme used in the technique.

$$AY\% = \frac{\text{Activity of immobilized enzyme}}{\text{Activity of free enzyme}} X\,100 \quad (2)$$

Immobilization efficiency was evaluated using Eq. (3)

$$IE\% = \frac{AY}{IY} X\,100 \quad (3)$$

Estimation of Enzyme Activity in Free Enzyme and Immobilized Samples

DNS method was employed for the determination of enzyme activity. Activity was studied on the basis of enzyme activity unit (EU). It is the amount of enzyme that catalyses the conversion of one micromole of substance per minute under optimized conditions of the assay method. A standard curve was drawn with different maltose concentrations. The reaction carried out in equal volumes of immobilized enzyme (0.5 mg/mL) and starch solution (1%) in desired buffer. It was then incubated at room temperature for nearly 15 min. The reaction was hindered by adding 1 mL 3,5-dinitrosalicylic acid reagent (DNS). Heated the reaction system in a boiling water bath for 5 min and cooled to room temperature. The amount of reduced sugar (maltose) produced was determined spectrophotometrically at 540 nm and compared the results with free enzyme[43].

Characterization of Immobilized Enzyme System Optimization Parameters for Immobilization

The pH at which the immobilized enzyme and free enzyme showed maximum activity were taken as its optimum value. It was determined for S1 and S2 by simply shaking the samples with starch around a pH of 4-9 at room temperature and compared the values with free enzyme. At maximum immobilization yield, the temperature of maximum activity was also determined at a set of 35-60°C. Next step is to check the thermal stability of free enzyme with immobilized enzymes and for that one should have free enzyme and immobilized enzymes with temperatures of order 35-60°C were pre-incubated for 1 hour in a water bath. After 1 hour of pre-incubation of both free and immobilized enzymes in selected buffer were cooled to room temperature and

catalytic reaction was performed with the addition of 1mL of 1 % starch solution to each reaction medium for an adequate time. Thermal inactivation curves with respect to incubation time for both free and immobilized enzymes were obtained by pre-incubating at different time intervals of 30-180 min. The refrigerated samples at 4ºC were taken for activity determination.

Quantitative Determination of Enzymatic Parameters

The maximum rate (V_{max}) and Michaelis constant (K_m) of starch hydrolysis for free and immobilised enzyme were evaluated by the means of Lineweaver-Burk plot. In order to conduct the experiment, different substrate concentrations ranges from 0.2-1.0 mg/mL were prepared. The immobilized enzyme was stirred with various starch concentrations in preferred buffer for 15 minute at room temperature and allowed to settle down precipitate. The cooled filtrate was taken for activity check. The reciprocal of Michaelis-Menton equation gives out a graph which is the Burk plot in which $1/V_o$ verses $1/S_o$ predicting the y-intercept as inverse of V_{max} and x-intercept as negative inverse of K_m.

Reusability and Storage Stability

The reusability of the immobilized enzymes were conducted at fixed time intervals or minimum of 8 cycles of repetitive usage of immobilized enzyme in fresh buffer solution. The relative activity of immobilized enzymes at optimized parameters were noticed every time at fixed time intervals. After each activity check, the used immobilized enzymes were removed and washed with fresh buffer solution followed by treating with new starch solution. It was continued for more number of cycles. The storage stability of immobilized enzymes were conducted by kept it in refrigerator for 6 weeks by maintaining the temperature at 4ºC in preferred buffer solution. The percentage relative activity of immobilized enzymes were compared with initial activity percentage.

Results and Discussion

Spectral Analysis of nanocomposites

The FT-IR spectra of MnO_2, NiO, CH, CH-MnO_2 and CH-NiO are shown (supplementary data-Appendix A). The absorption peak at 620 cm^{-1} was assigned to the Mn-O stretching vibration of MnO_2. The broad contour is observed due to the overlapping of the vibrational peaks. The band at 3430 cm^{-1} in MnO_2 spectrum is due to OH stretching vibration of adsorbed water. The less intense absorption peaks around 1671 cm^{-1} and 1084 cm^{-1} may be attributed to O-H bending vibrations combined with Mn atoms. The strong band around 400-450 cm^{-1} corresponds to the bending vibration of Ni–O bond. The broad absorption band centered at 3436 cm^{-1} is attributed to the O–H stretching vibrations, and the band at 1637 cm^{-1} is attributed to bending mode (H–O–H). The bands observed at 3436 cm^{-1} and the band in 1637 cm^{-1} are due to the fact that the calcined nanoparticles tends to physically absorb water and carbon dioxide from air. The FT-IR spectrum of pure CH has a peak at 3302 cm^{-1}. This peak represents the stretching vibration mode of $–NH_2$ and –OH groups. The band at 2907 cm^{-1} was attributed to the –CH group asymmetric stretching in polymer chain, 1646 cm^{-1} showed the amide I group, 1600 cm^{-1} was due to –NH deformation, 1402 cm^{-1} showed the amine group and 1083 cm^{-1} corresponds to the stretching vibration of C=O=C in glucose circle. The FT-IR spectrum of MnO_2-CH showed all the peaks shown by MnO_2 nanoparticles and chitosan. But we could observe some shifts in the IR values, only due to the formation of nanocomposite. Some structural differences must be observed during the formation of nanocomposite and resulted in peaks shifts. The peak at 3430 cm^{-1} due to the presence of O-H was shifted to 3386 cm^{-1}. Some more peaks were appeared at 1570 cm^{-1}, 1045 cm^{-1}, 1435 cm^{-1}, 850 cm^{-1} and 557 cm^{-1} were suggested the formation of nanocomposite. And the peak at 557 cm^{-1} confirmed the presence of nanoparticle MnO_2 on the CH surface. Peaks in between 426-620 cm^{-1} showed the NiO vibration band in the finger print region. Peaks around the region 1000-2200 cm^{-1} corresponds to the asymmetric and symmetric O-C=O stretching vibrations. Also the presence of C-O stretching vibration indicated the presence of NiO nanoparticles in the CH-NiO nanocomposite. The peaks at 3415 cm^{-1} showed the presence of O-H group and peaks at 1250-1650 cm^{-1} indicated the presence of amide bond, N-H in plane bending, C=O, C-H, C-N, structure again confirmed the presence of NiO on CH surface[39,43].

The nazo sized particles were distributed over the polymeric surface were clearly depicted from the SEM image. The synthesized MnO_2 nanoparticles were loosely distributed over the surface randomly. The morphology of the particles were nearly spherical and size of nanocomposite were increased only due to the electrostatic interaction. In some ares particles were seen to be agglomarated. The SEM image of the CH–NiO nanocomposite clearly revealed the granular rod shaped morphology of the NiO NPs in the CH network. The particles are in clustered form and they were agglomarated and packed randomly on the surface (supplementary data-Appendix B).

The X-ray diffraction data were recorded for the CH, as-prepared CH-MnO_2 and CH-NiO nanocomposites are depicted (supplementary data-Appendix C). The broad peak in the XRD pattern of CH at $2\theta=\sim20°$ represents the amorphous nature of biopolymer. . The peaks located at $2\theta = 29.09^0$, 37.68^0 and 56.99^0 represent the (310), (211) and (600) planes of tetragonal phase of α-type MnO_2. The average

crystalline size was determined from the Debye Scherrer equation,

$$D = K \lambda / \beta \cos \theta$$

Where D is the particle size, k is the Debye-Scherrer constant (0.89), λ is the wavelength of X-rays (0.15406 nm), β is the full width at half maximum and θ is the Bragg angle. It is found that the particles were of 22.8 nm for the plane (211) are distributed over the CH surface. dominant peaks exhibited for (111), (200) and (220) at 37.56^0, 43.58^0 and 63.157^0 respectively and the diffraction peak at (220) reveal the crystalline structure of NiO, the purity and crystallinity with the face-centered cubic configuration of 4.1Å and space group Fm3m (225). The three peaks corresponding to (111), (200) and (220) crystal planes indicated the formation of cubic nickel oxide. The other peak at 75.69^0 for (311) is corresponding to diffracting plane. The crystallite size of NiO is estimated from Debye Scherrer equation, 19.5 nm for the plane (111).

The TG and DTG curves of CH, CH-MnO_2 and CH-NiO are shown (supplementary data- Appendix D). There are two major weight loss peaks are observed for free chitosan. A decrease in weight at 72°C might be due to the moisture loss and other at 313°C due to thermal degradation of the CH polymer chains at elevated temperatures. CH-MnO_2 showed a decrease in weight around 90°C might be due to the moisture loss and a strong decrease in weight around 300°C due to thermal degradation of the low molecular weight oligosaccharides. Also showed a weight loss around 450-500°C may be due to the complete thermal decomposition of chitosan unit from the nanocomposite. Thermogram of CH-NiO showed four major weight losses at the points 77°C, 265°C, 432°C and 603°C. The weight loss around 77^0C may be due to the moisture loss. The thermal degradation of low-molecular weight polymeric chains of chitosan may be observed at 265°C. The complete degradation of chitosan unit from the nanocomposite may be observed at 432°C and the observed thermal stability of the nanocomposite is upto 600°C.

EDX analysis for the identification of metals and elements with high atomic percentages in nanocomposite are also shown (supplementary data-Appendix E).

Strategies of Optimization Process

The change in physical and chemical properties of enzyme as a result of immobilization must be affected by pH, temperature, contact time and concentration. The activity of enzyme should be expressed in relative activity, enzyme activity in the presence of factor over that in its absence. The effect of pH on immobilized enzyme present in the supernatant showed in figure 1a. Immobilization can bring about a shift in pH towards acidic or alkaline side and observed maximum immobilization yield for S1 and S2 at pH 6 and 7 respectively. The relative activity was measured at optimum pH conditions and could found a shift in the case of S2 from a pH 7 to pH 8 may be due to a net surface electrostatic interaction with the functional groups of CH with enzyme or due to the macromolecular feature of protein. Figure 1b predicted the effect of temperature on immobilized enzyme activity and immobilization yield was found to be 90% at 50ºC for S1 and 81% at 40ºC for S2. The relative activity for S1 and S2 were moved to 35ºC and 45ºC respectively due to desorption of enzyme from the support. As temperature goes up, enzyme undergoes denaturation. Figure 1c depicted the effect of contact time. The immobilization yield is 92% at 60 minute for S1 and 90.9% at 60 minute for S2. The optimum activity of enzyme is changed to 90 minute for both S1 and S2 due to lower accessibility of substrate as a result of multilayer adsorption of enzyme.

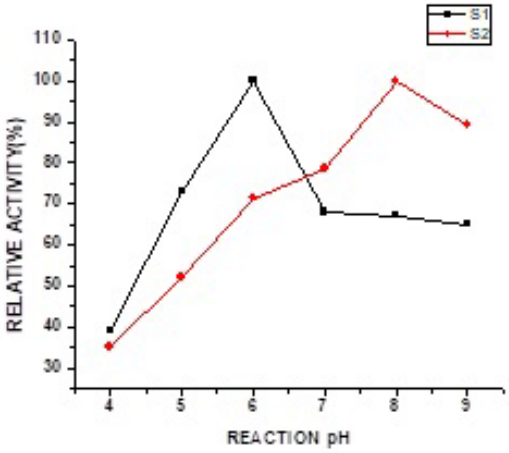

Figure 1a: Effect of pH on relative activity

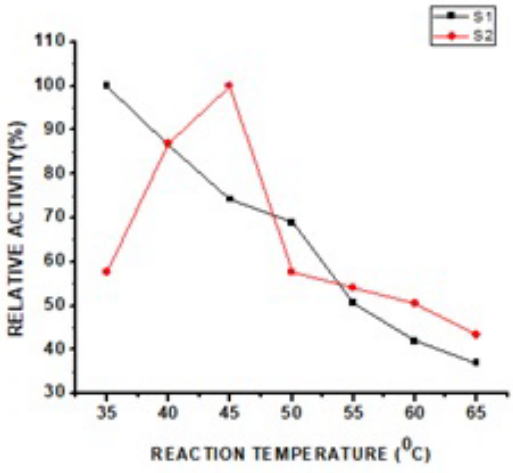

Figure 1b: Effect of temperature on relative activity

Finally the effect of protein concentration on relative activity was showed in figure 1d. Increasing substrate concentration increases the rate of reaction because more substrate molecules will be colliding with enzyme molecules, so more product will be formed. After a particular concentration, no further increase in adsorption occurs, a saturation point is reached and the enzyme start desorbed from the surface of the support. The protein loaded in S1 is found to be 85.7 % at a concentration of 0.4 mg and that of S2 is 90.9 % at a concentration of 0.4 mg respectively. The change in relative activity of S1 and S2 may be due to the aggregation of protein molecules. The results of immobilization yield, activity yield and immobilization efficiency were tabulated in table 1.

Table 1: Immobilization yeild, activity yield and immobilization efficiency of S1 and S2

Support	Initial protein (mg/mL)	Immobilized protein (mg/mL)	Immobilization yield (%)	Activity yield (%)	IE=AY/IY (%)
S1	0.40	0.20	85	48	56
S2	0.40	0.25	90	75	82

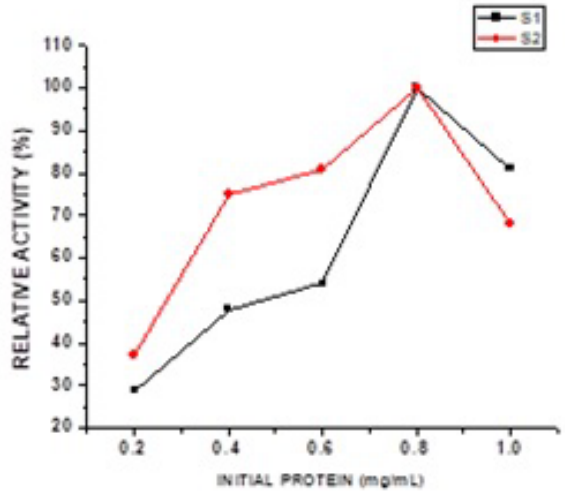

Figure 1c: Effect of contact time on relative activity

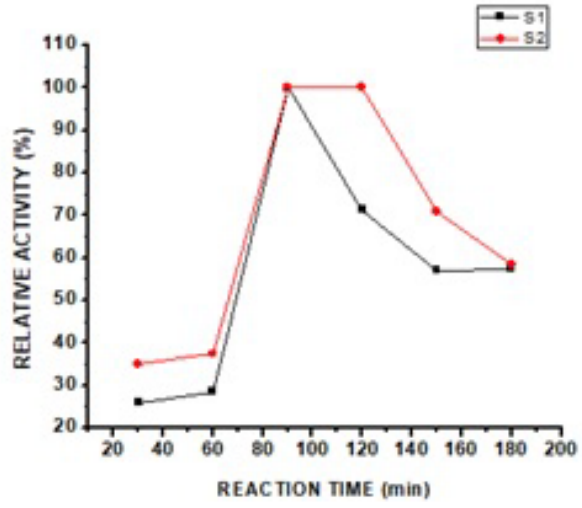

Figure 1d: Effect of concentration on relative activity

Determination of Properties of Free Enzyme and Immobilized Enzyme

Effect of pH on activity

Strong interactions of enzyme and supports resulted in a change in relative activity due to some conformational changes which must affects the intramolecular forces within enzyme conformation and stability of immobilized enzyme depends on optimum pH. The electrostatic interaction between functional groups on supports and enzyme shows maximum activity and thereby resulted in better immobilization efficiency. The effect of pH on relative activity and immobilization yield of immobilized α-amylase are determined in the pH range 4-9 and the results are shown in figure 2a. The optimal pH of free enzyme, α-amylase is 5.5 and free enzyme showed maximum activity at pH 6. Both supports showed maximum activity at alkaline pH region because of unequal separation of the cations and anions between the microenvironment of immobilized enzymes. The change in structural configuration or surface complexation may be the reason for variable pH values[44].

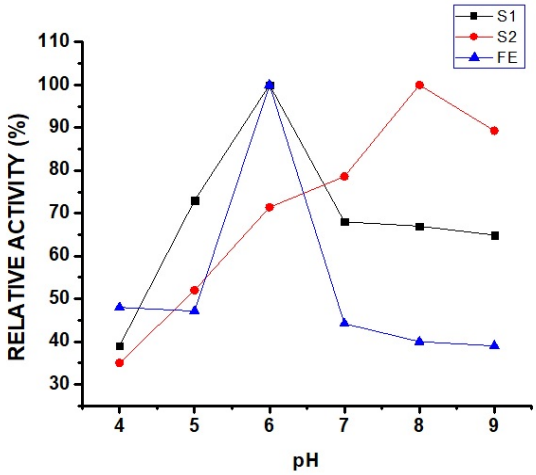

Figure 2a: Effect of pH on relative activity of free enzyme and supports

Effect of temperature on activity

Like most chemical reactions, the rate of an enzyme-catalyzed reaction increases as the temperature is raised. The rate reaches a maximum first and then tends to decreases. The decrease in rate at higher

temperature is due to denaturation of enzymes since the enzymes are highly sensitive. The effect of temperature on the enzyme activity of free enzyme and immobilized enzyme were studied by varying the temperature range 35°C-65°C. The optimum temperature of free enzyme is 50°C and showed optimum activity at 55°C. Relative activity for S1 and S2 were obtained at 35°C and 45°C respectively. The results are shown in figure 2b. The change in operational temperature was due to the changes in properties of enzyme as a result of immobilization. Existence of bond between support and enzyme have also reduced the conformational flexibility and there by resulted in behavioural changes. The decrease in activity of enzyme at longer temperatures were reported for some other chitosan based composites[45].

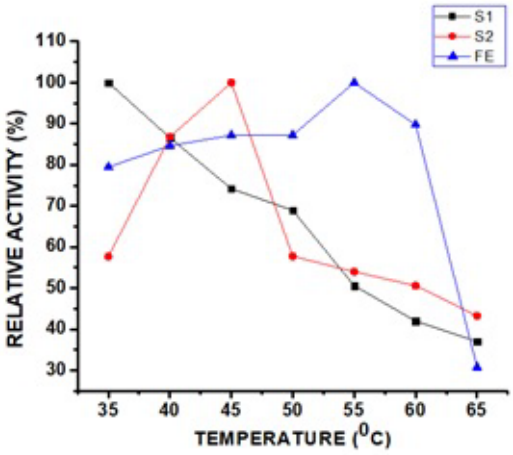

Figure 2b: Effect of temperature on relative activity of free enzyme and supports

In order to estimate the quantitative parameter activation energy (Ea), an Arrhenius plot was drawn between logarithms of relative activity (%) versus 1/T (figure 2c). The obtained values are 6.63, 12.60 and 7.18 KJ/mol for free enzyme, S1 and S2 respectively. The activation energy might be decreased for every cases due to the loss of conformational flexibility upon immobilization. A reported situation were seen in case of coconut fibre support[46].

Thermal stability and Thermal Inactivation

The main intuition of the present work is to shows that the enhanced thermal stability of enzymes upon immobilization and its finds greater goals in industries. The immobilized enzymes treated with preferred buffer solution and were pre-incubated from temperatures of 35ºC-65ºC. After 1 hour pre-incubation, at 60ºC the free enzyme has 26% relative activity and that of immobilized enzymes were around 50%. The results are shown in figure 2d. The immobilized enzyme, S1 and S2 exhibited better thermal stability on compared with free enzyme. Thermal inactivation were carried out in stable buffer and pre-incubated the free and immobilized enzymes at different time periods and depicted in figure 2e. The thermal inactivation must be a reason of protein unfolding that is restricted due to immobilization. Finally arrived at the statement that it preserves the tertiary structure of the enzyme and prevents enzyme vibration.

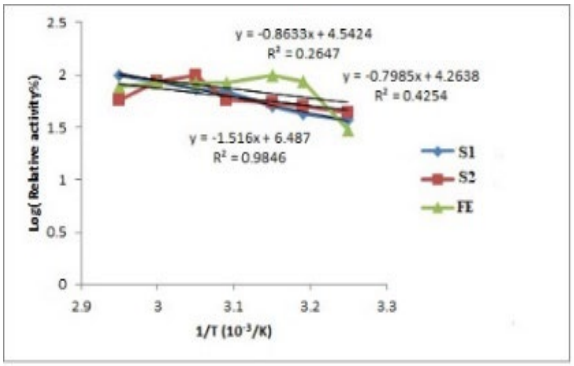

Figure 2c: Activation energy relationship with temperature for free and immobilized enzymes

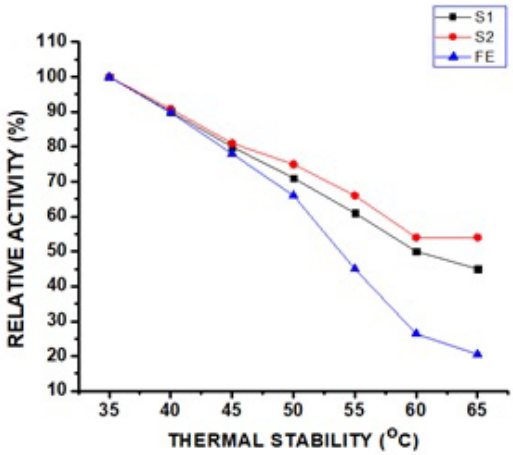

Figure 2d: Thermal stability at various temperatures

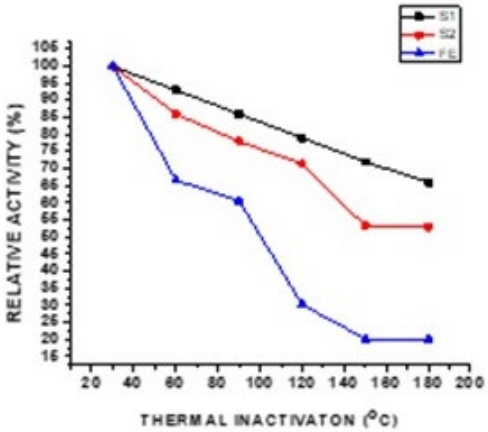

Figure 2e: Thermal inactivation at various contact times

Determination of Kinetic Parameters

The simple procedure for finding kinetic constants are using activity assay method and the substrate concentrations were varied from 0.2-1 mg/mL and arrived at the Michaelis-Menton equation on solving getting the Burk plot for quantitative parameters determination. The kinetic parameters for free and immobilized enzyme were calculated from Lineweaver-Burk (LB) plot. The parameters were estimated by using various substrate concentrations mentioned earlier. The K_m and V_{max} of immobilized form and free enzyme are not identical due to an affinity change for the substrate. Immobilization brought about an increase in the K_m value but a decrease in the V_{max}. Increase in K_m value suggested the requirement of higher substrate concentration and indicated the less porous structure. It also leads to lower accessibility of substrate to active site of immobilized enzyme. It suggests the lower affinity and conformational changes happened during immobilization technique. The decrease in V_{max} value was correlated with conformational changes thereby reduces the affinity to the substrate. Also read in terms of steric crowding of biological proteins caused by the diffusional limitation to supports[47]. The partial or complete inactivation of enzyme may lead to low value of V_{max}. The values of kinetic parameters are tabulated in table 2. The obtained LB plots are depicted in supplementary data (Appendix F).

Table 2: Kinetic parameters of free and immobilized enzyme

Kinetic parameters	Free enzyme	S1	S2
K_m (mg/mL)	1.2442	1.6303	1.2947
V_m (µmol mg^{-1} min^{-1})	69.9	54.0	44.8

Reusability and Storage Stability

The major challenge of enzyme immobilization is to enhance its reusability. Cost reduction is the crucial step while considering enzyme field so as to enhance the reusability by repeated batches of use of immobilized enzymes in stable buffer solutions. Immobilized enzymes were taken in stable buffer solutions mainly alkaline condition and kept at 4°C. Relative activity of immobilized enzymes was repeated for 8 times in fresh buffer solutions after each run. Immobilized enzyme, S1 retained 70% relative activity after 8 cycles and S2 retained 79% relative activity after 8 cycles (Figure 2f). Improved stability of immobilized enzyme can be attributed to the improved resistance to denaturation and conformational changes. The existence of strong bond may extend its stability. If the support exhibited magnetic property enzyme can be easily separated via magnetic methods. The reusability of immobilized α-amylase was investigated in several reports[48-50].

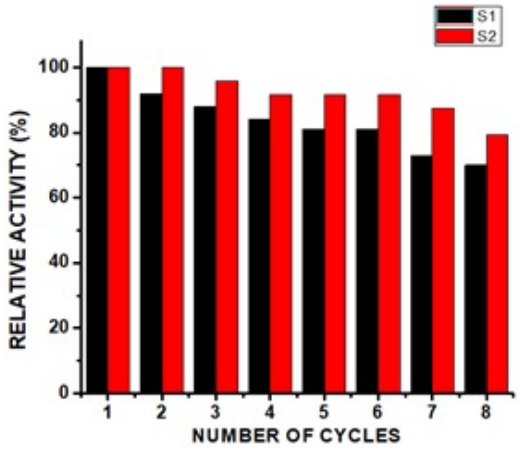

Figure 2f: Reusability of S1 and S2 for several reaction cycles

Free enzymes are sensitive with operational conditions. So storage of free enzyme will not extend upto weeks. In order to examine the storage stability of immobilized enzyme, it was stored at 4ºC for 6 weeks in buffer solution. Immobilized enzyme S1 retained 76% after 4 weeks and S2 retained 79% (Figure 2g). The results suggested that the immobilized enzyme exhibit improved storage stability. This is because conformational changes due to immobilization help the enzyme to suitably orient its active site towards the substrate. It limits the freedom to undergo drastic conformational changes and decrease in activity was explained as time-dependent natural loss in enzyme activity.

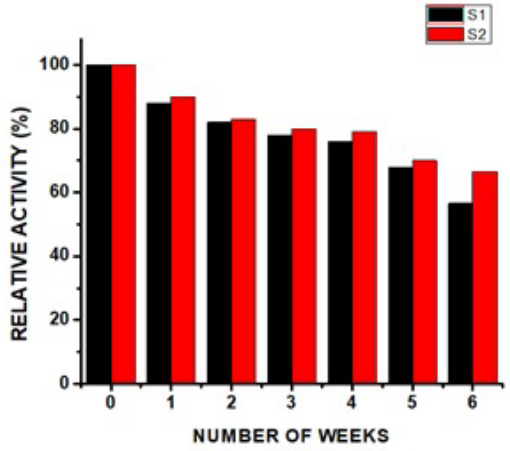

Figure 2g: Storage stability of S1 and S2 for longer period of days

Conclusion

Insoluble polymer based CH-MnO_2 and CH-NiO nanocomposites were synthesized successfully at laboratory. The formation of nanocomposites and presence of metals were confirmed via various characterisation techniques like FT-IR, FE-SEM, XRD, TGA, and EDX respectively. α-amylase enzyme was successfully immobilized onto the prepared supports S1 and S2. A convenient and easy technique was used for the immobilization. The immobilization parameters were optimised for S1 and S2. Properties of immobilized enzyme were carried out at optimised conditions. Enhancement in the thermal stability could be monitored. The activation energy of free enzyme was compared with immobilized enzymes. Evaluated the kinetic parameters and which showed that substrate affinity for the immobilized enzyme in enzymatic reaction is less and exhibited high K_m but low V_{max} compared to the free enzyme, indicate decreased activity. The reusability and storage stability of immobilized enzymes were improved. So both S1 and S2 can be widely employed in various industrial purposes.

Acknowledgments

The authors are thankful to UJRF for financial support and STIC, CUSAT for analyses.

References

1. Fishman A., Levy I., Cogan I. and Shoseyov O., Stabilization of horseradish peroxidase in aqueous-organic media by immobilization onto cellulose using a cellulose-binding-domain. *Journal of Molecular Catalysis B: Enzymatic*, 18(1–3): 121-131 (**2002**)
2. Altinkaynak C., Tavlasoglu S., Özdemir N. and Ocsoy I., A new generation approach in enzyme immobilization: Organic-inorganic hybrid nanoflowers with enhanced catalytic activity and stability. *Enzyme Microb. Technol*., 93–94: 105-112 (**2016**)
3. Mateo C., Palomo J.M., Fernandez-Lorente G., Guisan J.M. and Fernandez-Lafuente R., Improvement of enzyme activity, stability and selectivity via immobilization techniques. *Enzyme Microb. Technol*., 40(6): 1451-1463 (**2007**)
4. Doğaç Y.I., Deveci İ., Teke M. and Mercimek B., TiO_2 beads and TiO_2-chitosan beads for urease immobilization. *Mater. Sci. Eng. C. Mater Biol. Appl*., 42: 429-435 (**2014**)
5. Biró E., Németh A.S., Sisak C., Feczkó T. and Gyenis J., Preparation of chitosan particles suitable for enzyme immobilization. *J. Biochem. And Biophy. Methods*, 70: 1240-1246 (**2008**)
6. Cakmakcı E., Beyler Cigil A., Danıs O., Demir S. and Kahraman M., Immobilization of alpha-amylase on aminated polyimide membrane: Preparation, characterization, and properties. *Starch – Starke,* 66: 3-4, (**2014**)
7. Wang F., Gu Z., Cui Z. and. Liu L, Comparison of covalent immobilization of amylase on polystyrene pellets with pentaethylenehexamine and pentaethylene glycol spacers. *Bioresour. Technol*., 102(20): 9374-9379 (**2011**)
8. Cordeiro A.L., Lenk T. and Werner C., Immobilization of Bacillus licheniformis α-amylase onto reactive polymer films. ***J****. Biotechnol*., 154(4): 216-221 (**2011**)
9. Oktay B., Demir S. and Kayaman-Apohan N., Immobilization of α-amylase onto poly(glycidyl methacrylate) grafted electrospun fibers by ATRP. *Mat. Sci. Eng.* ***C****-Mater*., 50: 386-393 (**2015**)
10. Bindu V.U. and Mohanan P.V., Enhanced Stability of α-Amylase via Immobilization onto Chitosan-TiO_2. *Nanocomposite Nanosci. Technol*., 4(2):1-9 (**2017**)
11. Yang Y. and Chase H.A., Immobilization of α-amylase on poly (vinyl alcohol)-coated perfluoropolymer supports for use in enzyme reactors, *Biotechnol. Appl. BIioc*., 28(2): 145-154 (**1998**)
12. Kotwal S. M. and Shankar V., Immobilized invertase, *Biotechnol. Adv*., 27: 311-322 (**2009**)
13. Sheng Q., Luo K., Li L.and Zheng J., Direct electrochemistry of glucose oxidase immobilized on $NdPO_4$nanoparticles/chitosan composite film on glassy carbon electrodes and its biosensing application. *Bioelectrochem*., 74: 246–253 (**2009**)
14. Akamatsu K., Takei S., Mizuhata M., Kajinami A., Deki S., Takeoka S., Fujii M., Hayashi S. and Yamamoto K., Preparation and characterization of polymer thin films containing silver and silver sulfide nanoparticles. *Thin Solid Films*, 359: 55 (**2000**)
15. Zeng R, Rong M.Z., Zhang M.Q, Liang H.C. and Zeng H.M., Laser ablation of polymer-based silver nanocomposites. *Appl. Surf. Sci*., 187: 239 **(2002)**
16. Cole D. H., Shull K. R., Baldo P. and Rehn L., Dynamic Properties of a Model Polymer/Metal Nanocomposite. *Macromolecules*, 32: 771 **(1999)**
17. Hussain I., Brust M., Papworth A. J. and Cooper A. I., Preparation of Acrylate-Stabilized Gold and Silver Hydrosols and Gold-Polymer Composite Films. *Langmuir*, 19: 4831 (**2003**)
18. Kumar R.V., Elgamiel R., Diamant Y. and Gedanken A., Sonochemical Preparation and Characterization of Nanocrystalline Copper Oxide Embedded in Poly(vinyl alcohol) and Its Effect on Crystal Growth of Copper Oxide. *Langmuir*, 17: 1406 (**2001**)
19. Sajinovic D., Saponjic Z.V., Cvjeticanin N., Marinovic-Cincovic M. and Nedeljkovic J. M., Synthesis and characterization of CdS quantum dots–polystyrene composite. *Chem. Phys. Lett*., 329: 168 (**2000**)

20. Kumar R.V., Koltypin Y., Cohen Y.S., Aurbach D., Palchik O., Felner I. and Gedanken A., Preparation of amorphous magnetite nanoparticles embedded in polyvinyl alcohol using ultrasound radiation. *J. Mater. Chem*., 10: 1125 (**2000**)
21. Yu S.H., Yoshimura M., Moreno J.M.C., Fujiwara T., Fujino T. and Teranishi R., In Situ Fabrication and Optical Properties of a Novel Polystyrene/Semiconductor Nanocomposite Embedded with CdS Nanowires by a Soft Solution Processing Route. *Langmuir*, 17: 1700 (**2001**)
22. Mark J.E., Ceramic-reinforced polymers and polymer-modified ceramics. *Polym. Eng. Sci*., 36: 2905 (**1996**)
23. Zhao M. and Crooks M., Homogeneous Hydrogenation Catalysis with Monodisperse, Dendrimer-Encapsulated Pd and Pt Nanoparticles. *Angew. Chem. Int. Ed*., 38: 364 (**1999**)
24. Grohn F., Kim G., Bauer B.J. and Amis E.J., Nanoparticle Formation within Dendrimer-Containing Polymer Networks: Route to New Organic−Inorganic Hybrid Materials. *Macromolecules,* 34: 2179 (**2001**)
25. Kahn A., Koch N. and Gao W., Electronic structure and electronic properties of interfaces between metals and π-conjugated molecular films. *J. Polym. Sci. Polym. Phys*., 41: 2529-2548 (**2003**)
26. Shim I.W., Chol S., Noh W.T., Kwon J., Cho J.Y., Chae D.Y. and Kim K.S., Preparation of iron nanoparticles in cellulose acetate polymer and their reaction chemistry in the polymer. *Bull. Kor, Chem. Soc*., 22: 772 (**2001**)
27. Shim I.W., Noh W.T., Kwon J., Cho J.Y., Kim K.S. and Kang D.H., Preparation of copper nanoparticles in cellulose acetate polymer and the reaction chemistry of copper complexes in the polymer. *Bull. Kor, Chem. Soc*., 23: 563 (**2002**)
28. Nammalwar B., Fortenberry C., Bunce R.A., Lageshetty S.K. and Ausman K.D., Efficient oxidation of arylmethylene compounds using nano-MnO_2. *Tetrahedron Lett*., 54: 2010–2013 (**2013**)
29. Sun M., Lan B., Yu L., Ye F., Song W., He J., Diao G. and Zheng Y., Manganese oxides with different crystalline structures: Facile hydrothermal synthesis and catalytic activities. *Mater. Lett*., 86: 18–20 (**2012**)
30. Kamal T., Khan S.B. and Asiri A.M., Nickel nanoparticles-chitosan composite coated cellulose filter paper: An efficient and easily recoverable dip-catalyst for pollutants degradation. *Environ. Pollut*., 218: 625–633 **(2016)**
31. Awan I.Z., Hussain S.B., Ul Haq A. and Khan A.Q., Wondrous Nanotechnology. *J. Chem. Soc. Pak*., 38: 1026–1055 **(2016)**
32. Li Z., Sai H., Warren S.C., Kamperman M., Arora H., Gruner S.M. and Wiesner U., Metal Nanoparticle−Block Copolymer Composite Assembly and Disassembly. *Chem. Mater*., 21: 5578–5584 **(2009)**
33. Shah L.A., Ambreen J., Bibi I., Sayed M. and Siddiq M., Silver Nanoparticles Fabricated Hybrid Microgels for Optical and Catalytic Study. *J. Chem. Soc. Pak*., 38: 850–858 **(2016)**
34. Wan Ngah W.S., Teong L.C. and Hanafiah M.A.K.M., Adsorption of dyes and heavy metal ions by chitosan composites: A review. *Carbohydr. Polym*., 83: 1446–1456 **(2011)**
35. Mohan S., Srivastava P., Maheshwari S., Sundar S. and Prakash R., Nano-structured nickel oxide based DNA biosensor for detection of visceral leishmaniasis (Kala-azar). *Analyst*., 13: 2845–2851 **(2011)**
36. Ali M.A., Srivastava S., Solanki P.R., Reddy V., Agrawal V.V., Kim C., John R, and Malhotra B.D., Highly Efficient Bienzyme Functionalized Nanocomposite-Based Microfluidics Biosensor Platform for Biomedical Application. *Sci. Rep*., 3: 2661 (**2013**)
37. Bindu V.U. and Mohanan P.V., Enhanced stability of α-amylase via immobilization onto Chitosan-TiO_2 nanocomposite. *Nanosci. Technol*., 1-9, (**2017**)
38. Anwar Y., Antibacterial and lead ions adsorption characteristics of chitosan-manganese dioxide bionanocomposite. *Int. J. Biol. Macromol*., 111: 1140–1145 (**2018**)
39. Solanki P.R., Ali M.A., Agrawal V.V., Srivastava A., Kotnala R., Malhotra, Highly sensitive biofunctionalized nickel oxide nanowires for nanobiosensing applications. *RSC Adv*., 3(36): 16060–16067 (**2013**)
40. Farhadi S. and Roostaei-Zaniyani Z., Simple and low-temperature synthesis of NiO nanoparticles through solid-state thermal decomposition of the hexa(ammine)Ni(II) nitrate, $[Ni(NH_3)_6](NO_3)_2$, complex. *Polyhedron*, 30(7): 1244–1249 (**2011**)
41. Ali M.A., Solanki P.R., Patel M.K., Dhayani H., Agrawal V.V., John R. and Malhotra B.D., A highly efficient microfluidic nano biochip based on nanostructured nickel oxide. *Nanoscale*, 5(7): 2883–2891 (**2013**)
42. Solanki P.R., Patel M.K., Alic A. and Malhotra B D., A chitosan modified nickel oxide platform for biosensing applications. *J. Mater. Chem. B*., 3: 6698 (**2015**)
43. Pascoal A.M., Mitidieri S. and Fernandes K.F., Immobilisation of α-amylase from *Aspergillus niger* onto polyaniline, *Food Bioprod. Process*., 89(4): 300-306 (**2011**)
44. Tavano O.L., Fernandez-Lafuente R., Goulart A.J. and Monti R, Optimization of the immobilization of sweet potato amylase using glutaraldehyde-agarose support. Characterization of the immobilized enzyme. *Process Biochem*., 48(7): 1054-1058 (**2013**)

45. Chang M.Y. and Juang R.S., Activities, stabilities, and reaction kinetics of three free and chitosan–clay composite immobilized enzymes, *Enzyme Microb. Technol*., 36(1): 75-82 (**2005**)
46. Dey G., Palit S., Banerjee R. and Maiti B., Purification and characterization of maltooligosaccharide-forming amylase from Bacillus circulans GRS 313, *J. Ind. Microbiol. Biotechnol*., 28(4): 193-200 (**2002**)
47. Aksoy S., Tumturk H. and Hasirci N., Stability of α-amylase immobilized on poly(methyl methacrylate-acrylic acid) microspheres. *J. Biotechnol*., 60(1–2): 37-46 (**1998**)
48. Swarnalatha V., Esther R.A. and Dhamodharan R., Immobilization of α-amylase on gum acacia stabilized magnetite nanoparticles, an easily recoverable and reusable support. *J. Mol. Catal*., 96, 6-13 (**2013**)
49. Hasirci N., Aksoy S. and Tumturk H., Activation of poly(dimer acid-co-alkyl polyamine) particles for covalent immobilization of α-amylase, *React. Funct. Polym*., 66(12): 1546-1551 (**2006**)
50. Ashly P.C., Joseph M.J. and Mohanan P.V., Activity of diastase α-amylase immobilized on polyanilines (PANIs), *Food Chem*., 127(4): 1808-1813 (**2011**)